Electronic Supplementary Information

Dual Second Harmonic Generation and Up-Conversion Photoluminescence Emission in Highly-Optimized $LiNbO_3$ Nanocrystals Doped and Co-Doped with Er^{3+} and Yb^{3+}

K. Bredillet, F. Riporto, T. Guo, A. Dhouib, V. Multian, V. Monnier, P. Figueras Llussà, S. Beauquis, L. Bonacina, Y. Mugnier, R. Le Dantec

Table S1 *Summary table of the variable amounts of precursors used to prepare the set 1 of Er-doped samples with a varying molar concentration ranging from 1 to 6 mol %. The volume of niobium ethoxide is 308 µL for each synthesis and the total volume is adjusted at 10.3 mL with ethanol. The experimental content of Er derived from ICP-AES analysis is overall consistent with the theoretical one with the exception of only one value indicated in bold. The cell parameters and apparent crystallite sizes estimated along the [012], [110] and [006] directions from Le Bail refinements are also provided.*

Sample name	Er0% LN178	Er1% LN215	Er2% LN216	Er3% LN217	Er4% LN218	Er5% LN219	Er6% LN220
Lithium ethoxide volume (µL)	1200	1164	1128	1092	1056	1020	984
Erbium isopropoxide Mass (mg)	0	4.1	8.2	12.3	16.4	20.5	24.6
mol % of Er from ICP-AES	0	0.6	2.2	2.4	**2.3**	4.0	5.7 Not phase pure
Size [012] (nm)	21	24	19	19	16	18	15
Size [110] (nm)	45	45	31	31	23	27	18
Size [006] (nm)	14	17	14	14	13	14	14
A (Å)	5.14507(5)	5.14554(5)	5.1469(1)	5.14696(6)	5.14527(7)	5.14670(6)	5.14309(9)
c (Å)	13.8868(2)	13.8913(2)	13.8903(3)	13.8939(3)	13.8899(3)	13.8875(3)	13.8955(3)

Table S2 *Summary table of the variable amounts of precursors used to prepare the set 2 of Er-doped samples with a varying molar concentration ranging from 1 to 6 mol %. The volume of niobium ethoxide is 308 µL for each synthesis and the total volume is adjusted at 10.3 mL with ethanol. The experimental content of Er derived from ICP-AES analysis is overall consistent with the theoretical one with the exception of only one value indicated in bold. The cell parameters and apparent crystallite sizes estimated along the [012], [110] and [006] directions from Le Bail refinements are also provided.*

Sample name	Er1% LN204	Er2.5% LN207	Er3% LN196	Er4% LN198	Er6% LN201
Lithium ethoxide volume (µL)	1164	1128	1092	1056	984
Erbium isopropoxide Mass (mg)	4.1	8.2	12.3	16.4	24.6
mol % of Er from ICP-AES	1.0	**0.6**	2.8	3.8	5.2
Size [012] (nm)	18	17	22	19	16
Size [110] (nm)	30	22	38	29	20
Size [006] (nm)	14	14	16	14	13
A (Å)	5.14616(8)	5.14209(8)	5.14605(5)	5.14811(5)	5.1445(1)
c (Å)	13.8933(4)	13.8902(3)	13.8895(2)	13.8831(2)	13.8939(4)

Table S3 *Summary table of the variable amounts of precursors used to prepare Er/Yb co-doped samples with a varying molar concentration of lanthanide ions ranging from 2.4 to 8.4 mol %. The volume of niobium ethoxide is 308 µL for each synthesis and the total volume is adjusted at 10.3 mL with ethanol. The experimental molar content of Er and Yb derived from ICP-AES analysis is also indicated together with the cell parameters and apparent crystallite sizes estimated along the [012], [110] and [006] directions from Le Bail refinements (only for phase-pure samples)*

Sample name	Er0,4%-Yb2% LN108	Er0,6%-Yb3% LN98	Er0,8%-Yb4% LN131	Er1,0%-Yb5% LN154	Er1,2%-Yb6% LN144	Er1,4%-Yb7% LN145	Er3%-Yb3% LN152
Lithium Ethoxide Volume (µL)	1110	1070	1030	985	941	898	985
Erbium Isopropoxide Mass	1,65mg	2,5mg	3,3mg	4,1mg	4,9mg	5,7mg	12,3mg
Ytterbium Isopropoxide Mass	8,4mg	12,6mg	16,8mg	21mg	25,2mg	29,4mg	12,6mg
mol % of (Er/Yb) from ICP-AES	(0.5/2.0)	(1.1/2.3)	(1.0/4.0)	(0.3/4.4)	Not phase pure	(0.9/7.3) Not phase pure	(2.9/2.5)
Size [012] (nm)	18	15	16	15			16
Size [110] (nm)	30	24	23	22			23
Size [006] (nm)	13	11	13	12			12
A (Å)	5.14811(7)	5.1496(1)	5.14919(6)	5.14651(9)			5.1472(4)
c (Å)	13.8939(3)	13.8997(3)	13.8925(2)	13.8927(4)			13.8969(3)

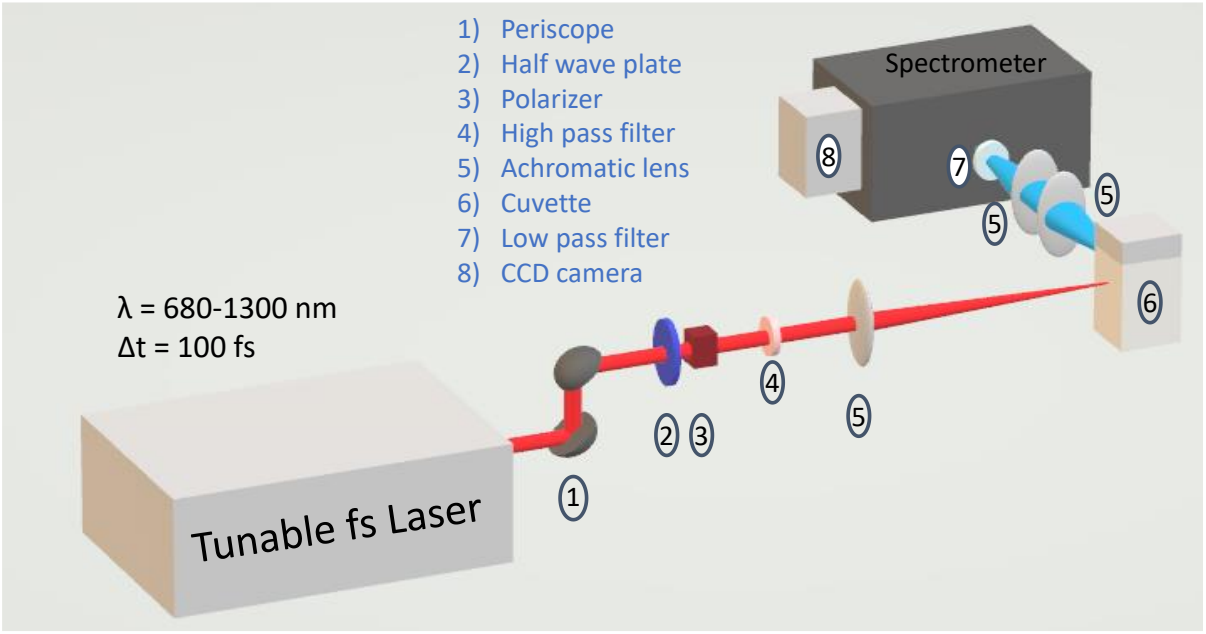

Fig. S1 *Scheme of the optical setup used for second harmonic scattering and up-conversion photoluminescence measurements.*

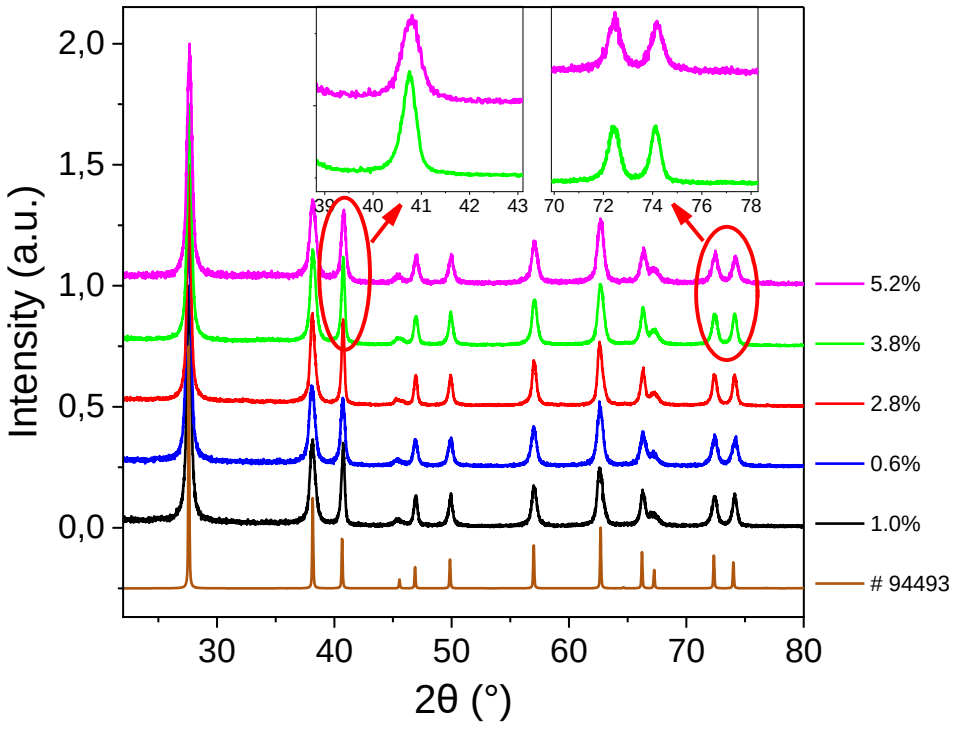

Fig. S2 *X-Ray diffraction profiles of the second series of samples of Table S2 showing the absence of any phase impurity till the highest content of Er measured at 5.2 mol %.*

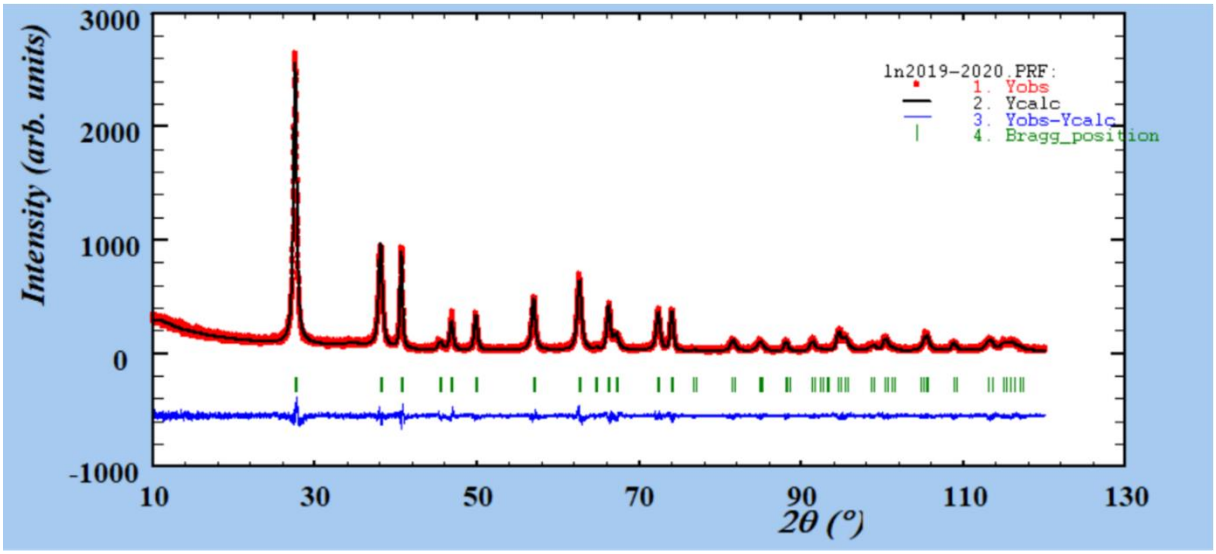

Fig. S3 *Example of Le Bail fit refinement for LN nanocrystals doped with 4 mol % of Er^{3+} resulting in a global chi2 value at 1.47 and the apparent crystallite sizes and cell parameters mentioned in Table S1.*

Representative TEM images and associated size distributions for the doped and co-doped samples

LN 215, 0.6 mol % of Er

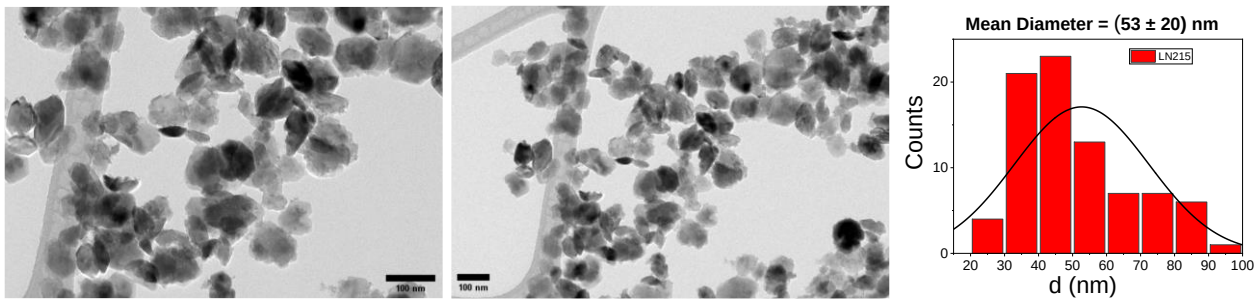

LN 219, 4 mol % of Er

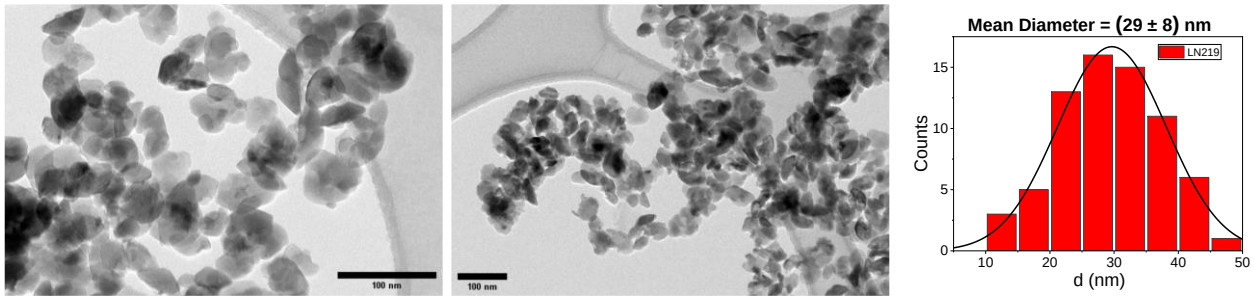

LN 198, 3.8 mol % of Er

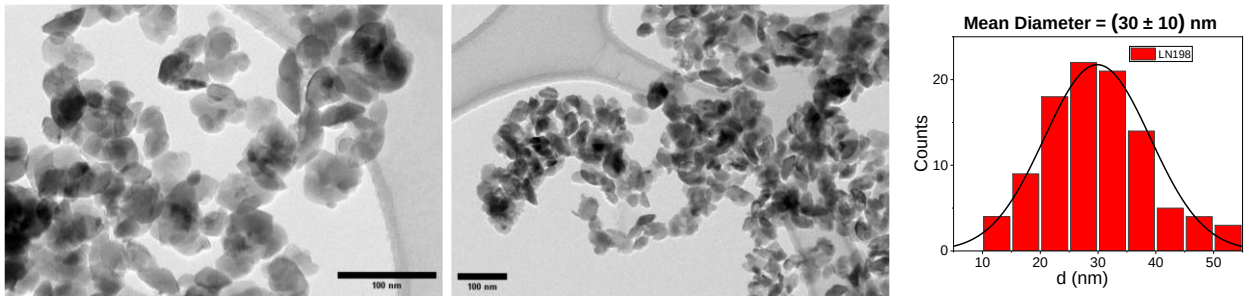

LN 131, 1.0 mol % of Er and 4.0 mol % of Yb

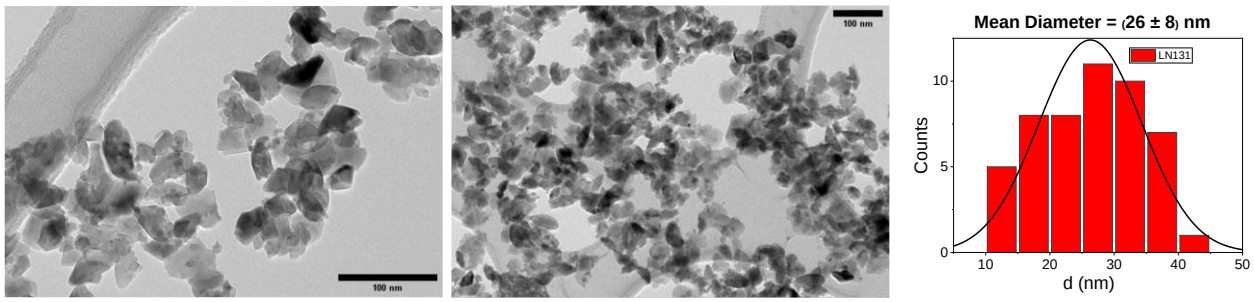

LN 152, 2.9 mol % of Er and 2.5 mol % of Yb

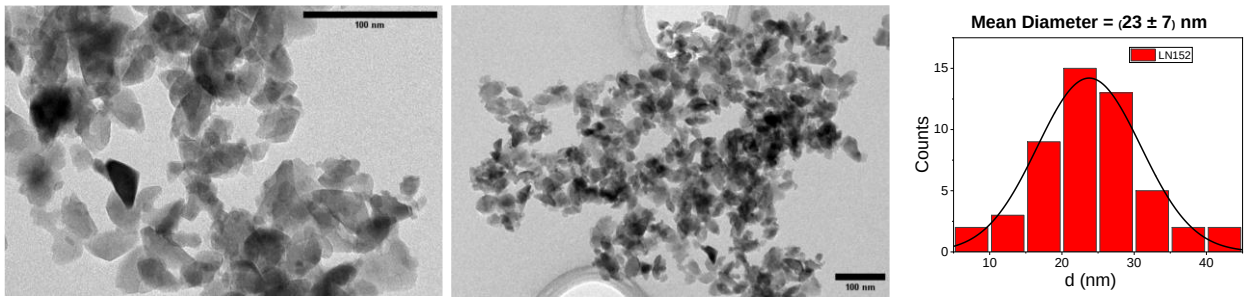

Fig. S4 *Representative TEM images of the main samples of interest and corresponding size distributions obtained from 50-100 individual nanocrystals. Note that, with the exception of sample LN215 (0.6 mol % of Er), the mean size is always at about 25-30 nm and with a standard deviation below 10 nm. The mean sizes are very consistent with the ones obtained in Tables S1-S3 from Le Bail refinements since a given size distribution is to be considered along each [hkl] direction.*

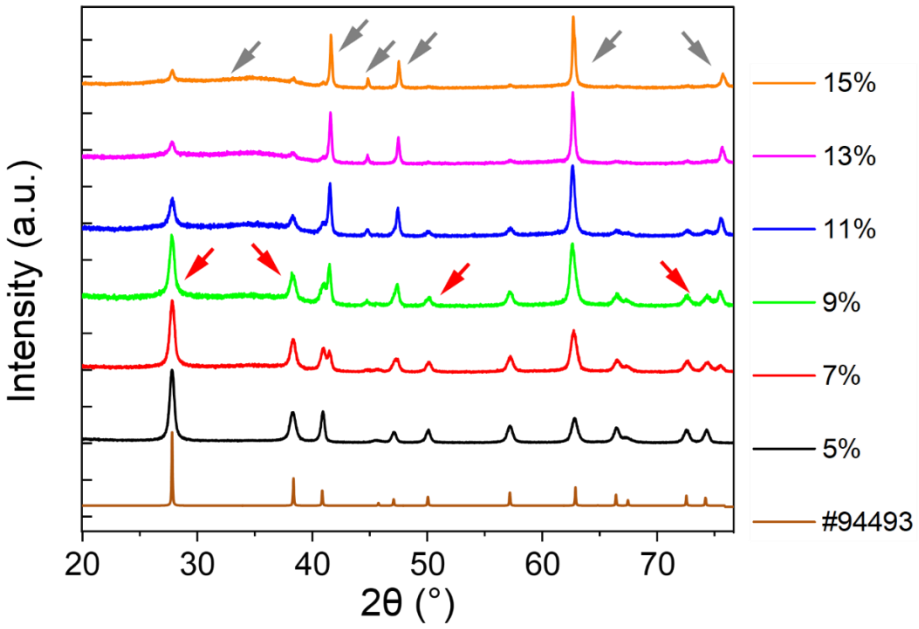

Fig. S5 *X-Ray diffraction profiles of powders prepared with an increasing theoretical erbium content varying from 5 mol % to 15 mol %. Red arrows indicate the progressive disappearance of some broad reflections associated with LN nanocrystals while grey arrows correspond to new, thinner diffraction peaks of a supposedly Nb-rich phase and to an increasing background around 35° in 2θ.*

Up-conversion mechanisms leading to the photoluminescence emission when excited at 800 nm and 980 nm

800 nm excitation

Various mechanisms can be involved to populate the $^2H_{11/2}$ and $^4S_{3/2}$ emitting levels, which are responsible for the emissions at 525 and 550 nm, respectively (Fig. S6). A first ground state absorption (GSA) allows excitation of the $^4I_{9/2}$ state (12500 cm^{-1}). As recently discussed,[1] two mechanisms either based on excited state absorption (ESA) or on cross-relaxation by Energy Transfer (ET) between two neighbouring Er^{3+} ions, can lead to the green UC-PL signals. For the ESA hypothesis, a non-radiative de-excitation occurs between $^4I_{9/2}$ and $^4I_{11/2}$ before a second absorption. Levels $^4F_{3/2}$ and $^4F_{5/2}$ are then populated (as described by ESA 1 in Fig. S6) before new non-radiative de-excitations towards the $^2H_{11/2}$ and $^4S_{3/2}$ levels. Another possibility is the ESA 2 mechanism implying non-radiative de-excitations from $^4I_{9/2}$ to $^4I_{11/2}$ and to $^4I_{13/2}$ after the initial GSA. The second absorption then corresponds to $^4I_{13/2} \rightarrow {}^2H_{11/2}$ and again involves only one Er^{3+} ion. Conversely, two nearby Er^{3+} ions can interact through two different ET mechanisms. The first one, denoted as ET 1, can be described as $^4I_{11/2} + {}^4I_{11/2} \rightarrow {}^4F_{7/2} + {}^4I_{15/2}$ and is followed by a non-radiative de-excitation from $^4F_{7/2}$ to the $^2H_{11/2}$ and $^4S_{3/2}$ emitting levels. The second energy transfer is labelled as ET 2 and corresponds to $^4I_{11/2} + {}^4I_{13/2} \rightarrow {}^2H_{11/2} + {}^4I_{15/2}$.

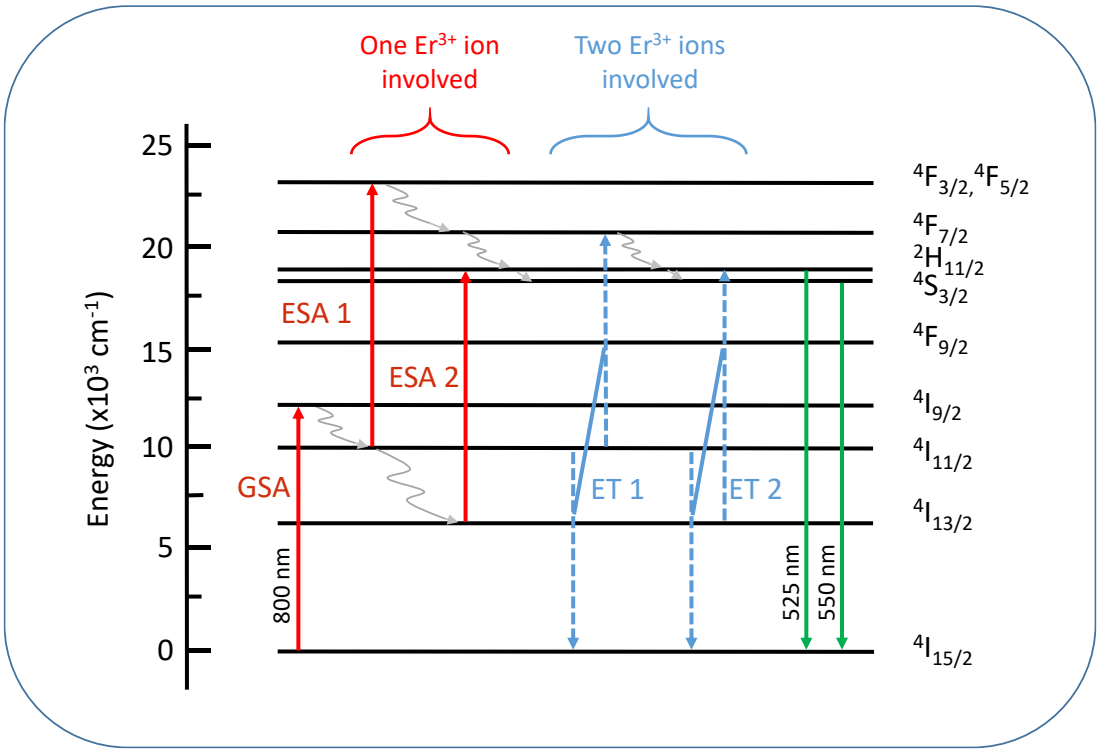

Fig. S6 *Energy level diagram of the possible up-conversion processes leading to the green photoluminescence emissions at 525 and 550 nm when excited at 800 nm.*

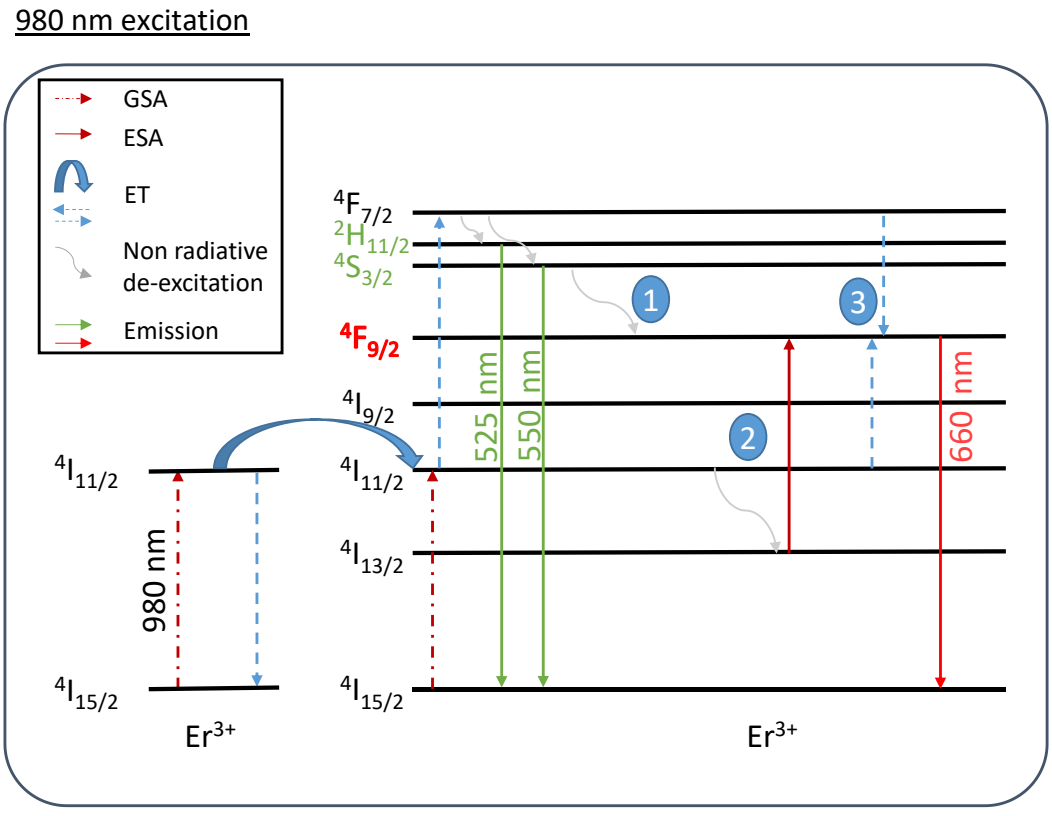

Fig. S7 *Energy level diagram of the up-conversion processes leading to the green and red photoluminescence emissions at 525, 550 and 660 nm when excited at 980 nm.*

With the excitation set at 980 nm, the green and red emitting levels can be populated by well-documented up-conversion processes.[2–4] After the initial GSA (Fig S7), the $^4F_{7/2}$ excited state of the emitting Er^{3+} ion is either populated by ESA or ET from another nearby erbium ion. In both cases, non-radiative de-excitations occur between $^4F_{7/2}$ and the $^2H_{11/2}$ and $^4S_{3/2}$ green emitting levels.

Regarding the red UC-PL emission, three hypotheses labelled as 1, 2 and 3 in Fig S7 can be put forward. The first is based on non-radiative de-excitation from the $^4S_{3/2}$ state to the $^4F_{9/2}$ emitting level. The second suggests that a non-radiative de-excitation takes place between $^4I_{11/2}$ and $^4I_{13/2}$ before excitation of the $^4F_{9/2}$ state from ESA. Finally, the last involves the excited states of two different erbium ions, namely $^4I_{11/2}$ and $^4F_{7/2}$, after absorption of one and two photons, respectively. The energy transfer $^4I_{11/2}$ + $^4F_{7/2}$ -> 2 $^4F_{9/2}$ is then postulated to explain population of the red emitting level.

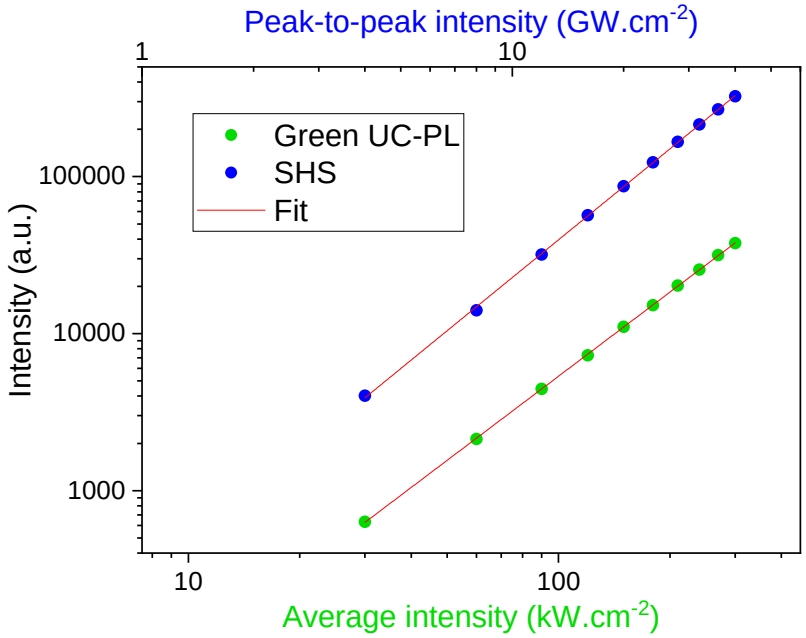

Fig. S8 *LN:4.0%Er^{3+} power law dependences excited at 800 nm corresponding to the SHG (blue dots, 400 nm) and UC-PL emissions (green dots, 525 and 550 nm). Data are plotted in log-log scale and the linear fits (red lines) are performed using the function $y=A.x^n$ with n the non-linear free index experimentally derived for each optical process.*

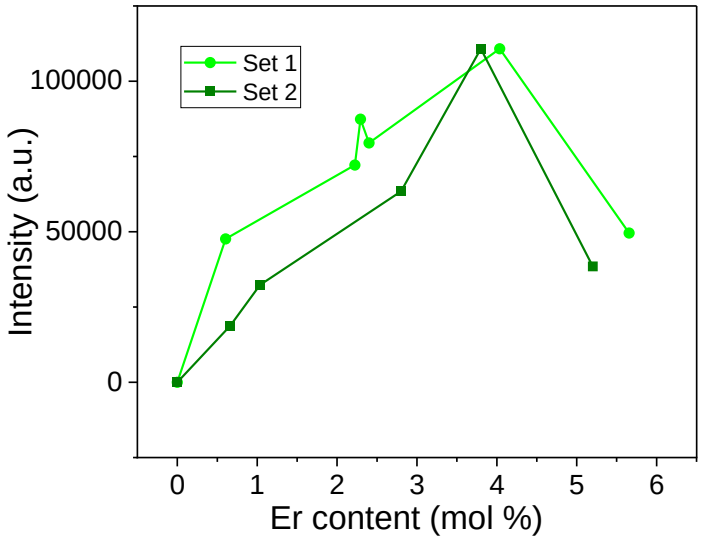

Fig. S9 *Comparison between the green UC-PL intensities measured from nanocrystal suspensions prepared from for the two different sets of samples and for which the experimental molar concentration in erbium is summarized above in Tables S1 and S2.*

Up-conversion mechanisms leading to the green and red photoluminescence emissions in Er^{3+}/Yb^{3+} co-doped $LiNbO_3$ nanocrystals when excited at 980 nm

Energy transfer (ET) between Yb^{3+} and Er^{3+}

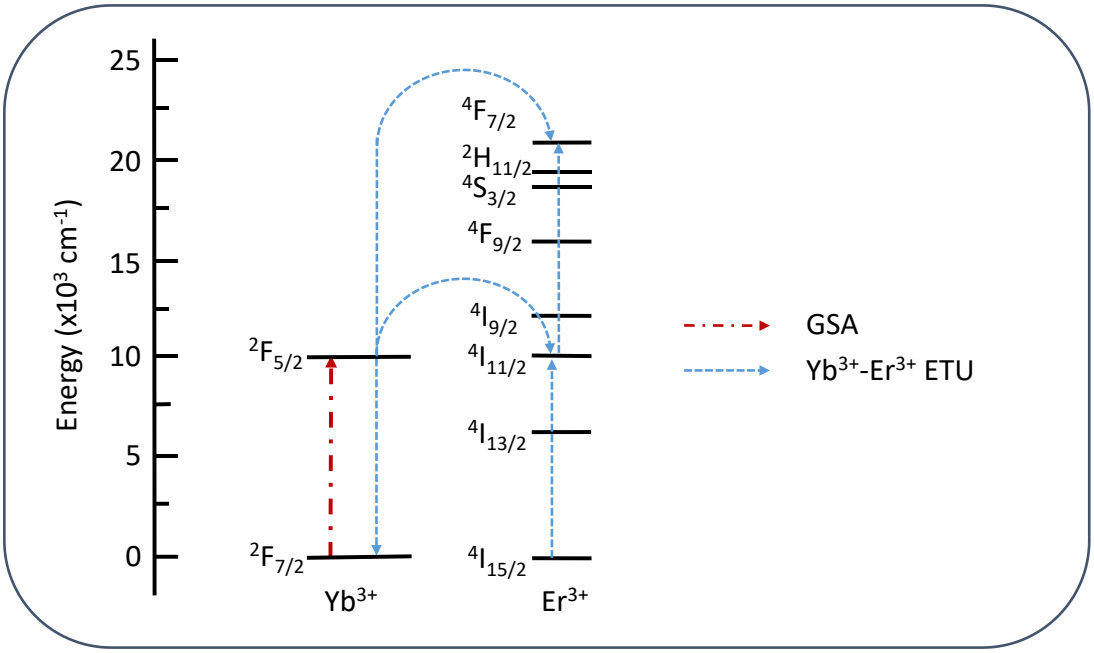

Fig. S10 *Energy transfer up-conversion for Yb^{3+}-Er^{3+} couple*

Ytterbium ions are added to the structure for their high effective absorption cross-section at 980 nm. They enable the absorption process to be enhanced and then transfer their

energy to neighbouring erbium ions. This is made possible by the very close energy levels $^2F_{5/2}$ of ytterbium and $^4I_{11/2}$ of erbium (around 10 000 cm^{-1}). The up-conversion mechanisms leading to green and red photoluminescence emissions are then similar to those presented for erbium-doped particles.

XRD phase purity of co-doped LN nanocrystals as a function of the total concentration of Er^{3+} and Yb^{3+} ions.

As discussed in the main text for Er-doped samples, the doping limit is also investigated for Er/Yb co-doped nanocrystals prepared from a varying molar concentration of lanthanide ions ranging from 2.4 to 8.4 mol %. The Yb/Er ratio is here fixed in Fig S11 at 5. Given that both Er and Yb ions enter the LN host near the lithium site, the total concentration in lanthanide ions is to be considered as already outlined in bulk crystals.[5] In good agreement with the XRD characterizations of the Er mono-doped samples illustrated in Fig 1a, the same impurity phase and apparition of a significant background are evidenced in Fig S11 when the total dopant content exceeds 6 mol %. The doping limit for XRD phase-pure co-doped nanocrystals is thus again found at about 5 mol % according to the chemical analyses provided in Table S3.

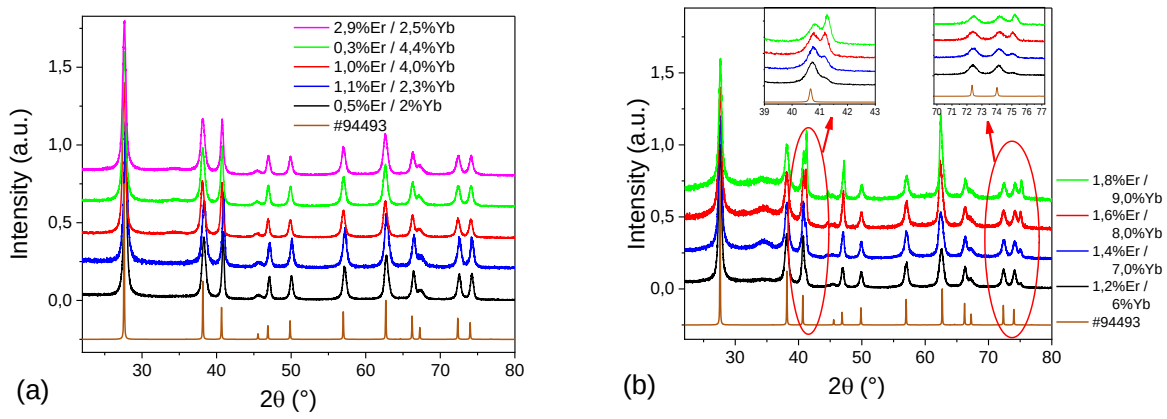

Fig. S11 *X-Ray diffraction profiles of samples prepared at a total lanthanide content varying from 2.4 to 9.8 mol % and for a Yb/Er ratio fixed at 5. (a) XRD phase-pure samples of Table S3 for which the experimental concentrations in Er^{3+} and Yb^{3+} ions are known. (b) Additional samples prepared with a total lanthanide content above 7.2 mol % for which the chemical analyses have not been performed because of the obvious presence of the same impurity phase already detected in Figures 1a, S2 and S4 when the initial Er content was fixed above 6 mol %.*

References

1 D. Sola, A. Miguel, E. Arias-Egido and J. I. Peña, *Applied Sciences*, 2021, **11**, 1137.
2 J. J. Ju, T. Y. Kwon, S. I. Yun, M. Cha and H. J. Seo, *Applied Physics Letters*, 1996, **69**, 1358–1360.
3 F. Wang and X. Liu, *Chem. Soc. Rev.*, 2009, **38**, 976.
4 A. Nadort, J. Zhao and E. M. Goldys, *Nanoscale*, 2016, **8**, 13099–13130.
5 E. Cantelar and J. A. Sanz-Garc, *Journal of Crystal Growth*, 1999, **205**, 196–201.